Submitted to the International Europhysics Conference on High Energy Physics HEP99,
Tampere, Finland, July 1999

First Measurement of Three Jet Cross Sections in DIS at HERA

H1 Collaboration

Abstract

The production of three jets with high transverse momentum has been studied in deep inelastic positron-proton scattering with the H1 detector at HERA. Jets are defined by the inclusive k_T algorithm in the Breit frame.

Cross sections as a function of the squared transferred 4-momentum Q^2, the Bjorken scaling variable x_{Bj} , the mean transverse energy $\overline{E}_{T,\mathrm{Breit}}$ and the invariant mass M_{3jet} of the three jets have been measured over a wide Q^2 range from 5 to $5000\ \mathrm{GeV}^2$. Moreover, the ratio of the three jet cross section with respect to the two jet cross section $R_{3/2}$ has been measured as a function of Q^2 and the mass of the hard process M_{njet} for $Q^2 > 150$ GeV^2 and $M_{\mathrm{njet}} > 25$ GeV.

The shape of the Dalitz variables $X_3 = 2\,E_3/M_{\mathrm{3jet}}$, $X_4 = 2\,E_4/M_{\mathrm{3jet}}$, where E_3 (E_4) is the energy of the (second) highest energetic jet in the three jet rest frame, and two angular distributions characterising the angular orientation of the jets are studied. The data are compared to $\mathcal{O}(\alpha_s^2)$ perturbative QCD (pQCD) calculations and to QCD Monte Carlo models. $\mathcal{O}(\alpha_s^2)$ pQCD calculations describe the data well for $Q^2 \gtrsim 40\ \mathrm{GeV}^2$ and for transverse jet energies $\overline{E}_{T,\mathrm{Breit}} > 10$ GeV. For lower Q^2 and lower E_T they fall below the data. Monte Carlo models have difficulties in describing the cross sections, but are able to reproduce the shape normalised angular distributions in the three jet centre of mass system. The jet with the lowest energy in the three jet centre of mass frame is most likely to be emitted in the direction of the proton beam. This contrasts with a uniform distribution of the available phase space, but it is consistent with the observation that in the QCD models this jet mainly stems from initial state radiation processes.

Abstract: 157
Parallel sessions: 1
Plenary sessions: 1

1 Introduction

The large centre of mass energy of HERA colliding 27.5 GeV positrons on 820 GeV protons offers an ideal testing ground for the production mechanism of strongly interacting hadrons in deep-inelastic scattering (DIS). The properties of the strong interactions can be studied at short distances in the presence of two hard scales: the virtuality of the exchanged photon Q^2 and the transverse energy E_T produced in the hard scattering. In a reference frame, where the virtual photon interacts head-on with the proton, like the Breit frame[1], the transverse energy directly reflects the hardness of the underlying process.

Within the context of the theory of the strong interaction (QCD), hard processes can be described as the point-like scattering between the virtual photon and the constituent partons of the proton. The scattering cross section can be written as a convolution of perturbative coefficients expanded in powers of the strong coupling constant α_s and the parton momentum distributions inside the proton. In leading order of α_s gluon and quark initiated processes lead to two partons in the final state. Terms to order α_s^2 produce processes with three partons. The coloured partons evolve from the hard scattering via soft parton radiation and hadronisation processes to the collimated sprays of observable hadrons, called jets.

In [1] it has been shown that inclusive dijet cross sections in the Breit frame over a large kinematic domain from $10 < Q^2 < 5000\ \mathrm{GeV}^2$ are successfully described by $\mathcal{O}(\alpha_s^2)$ pQCD calculations. For this observable $\mathcal{O}(\alpha_s^2)$ is next-to-leading order (NLO) in the perturbative expansion. In this analysis for the first time measurements of inclusive three jet cross sections in deep-inelastic scattering are presented and compared to tree-level pQCD calculations ($\mathcal{O}(\alpha_s^2)$) and QCD Monte Carlo models. Furthermore, the topology of the jets in their rest frame is investigated. These measurements test the validity of pQCD for three jet configurations.

The properties of multijet events in reactions with strongly interacting particles in the initial state have been previously studied in $p\bar{p}$ collisions at the SPS [2, 3] and at the TEVATRON [4–7]. At HERA, first measurements have been performed in collisions of real photons with the proton [8].

2 Selection of DIS Events

The data presented in this paper are obtained in two different kinematic ranges of the squared four momentum transfer Q^2 going from 5 to $100\ \mathrm{GeV}^2$ and from 150 to $5000\ \mathrm{GeV}^2$. The data selection is described in two parts accordingly.

2.1 Selection of the Low Q^2 DIS events

This sample is based on H1 data taken in 1997 corresponding to an integrated luminosity of $\mathcal{L}_{int} = 15.6$ pb^{-1}. Events with a scattered positron of at least 8 GeV in the acceptance region of

[1]The Breit frame is defined by $\vec{q} + 2x_{\mathrm{Bj}}\vec{P} = 0$, where $\vec{q}$ and $\vec{P}$ are the momenta of the exchanged boson and the incoming proton. The z-axis is defined as the direction of the incoming proton.

the backward calorimeter (SpaCal) are selected covering positron polar angles $177.8° < \theta_{el} < 153°$. An energy deposit of at least 6 GeV and a loose track requirement is required on the trigger level.

The hadronic final state used as input to the jet algorithm consists of energy deposits from the SpaCal and LAr calorimeter and track momenta measured in the central tracker as input to the jet algorithm. While all energy clusters are considered, the four momentum of each single track is only allowed to contribute up to a momentum of $300\,\mathrm{MeV}$. This procedure closely follows the one used in [9,10].

The DIS sample is defined by applying the following cuts:

- The polar angle of the scattered positron is restricted to $\theta_{el} > 156°$.
- Q^2 is required to be in the range $5 < Q^2 < 100\ \mathrm{GeV}^2$.
- The inelasticity $y = Q^2/(x_{Bj}\ s)$ is restricted to 0.2 < y < 0.6 where $\sqrt{s} \approx 300$ GeV is the positron-proton centre-of-mass energy and x_{Bj} the Bjorken scaling variable defined by $x_{Bj} = Q^2/(2Pq)$.
- The position of the z coordinate of the reconstructed event vertex must be within ± 35 cm of the nominal position.
- A cut on $35 < \sum(E - p_z) < 70\,\mathrm{GeV}$ is applied, where the sum runs over all energy depositions in the SpaCal and LAr calorimeters.

2.2 Selection of High Q^2 DIS events

This sample is based on H1 data taken in $1995-1997$ corresponding to an integrated luminosity of $\mathcal{L}_{int} \approx 33$ pb^{-1}. Events with the scattered positron with an energy of at least 11 GeV in the acceptance region of the liquid argon calorimeter are selected covering $4° < \theta_{el} < 154°$. On the trigger level, an electromagnetic energy deposit of at least 6 GeV is required in a coarsely segmented tower pointing to the interaction vertex.

The hadronic final state used as input to the jet algorithm consists of low momentum tracks ($p_T < 2$ GeV) and energy deposits in the SpaCal and LAr calorimeter is used. To avoid double counting of the energy, the energy measured in the electromagnetic (hadronic) calorimeter in a cylinder of 15 (25) cm in radius around the axis given by the direction of the track is not taken into account. If, however, the total energy in the cylinder is greater than the energy of the track, only the calorimeter information is counted. This procedure has also been used in [11].

The DIS sample is defined by applying the following cuts:

- The impact point of the scattered positron is required to be $z_{track,el} > -180$ cm. Inactive regions between the wheels and in between the octants are removed from the analysis.
- Q^2 is required to be $150 < Q^2 < 5000\ \mathrm{GeV}^2$.

- The inelasticity $y = Q^2 \,/(x_{Bj}\, s)$ is restricted to be 0.2 < y < 0.6.
- The position of the z coordinate of the reconstructed event vertex must be within ± 35 cm of the nominal position.
- A cut on $45\,\mathrm{GeV} < \sum(E - p_z) < 65\,\mathrm{GeV}$ is applied, where the sum runs over a combination of low transverse momentum tracks ($p_t < 2$ GeV) and energy deposits in the SpaCal and LAr calorimeters (see section 3).

For both data samples, the contamination by events with misidentified positrons stemming from real γp reactions is negligible, i.e. $\lesssim 2\%$. This has been estimated by the Monte Carlo simulation program PHOJET [12].

3 Selection of Three Jet Events

Jets are defined in the Breit frame by the inclusive k_T algorithm [13, 14] which is applied to all particles. Particle refers either to an energy deposit in the detector, to a stable hadron or to a parton in a QCD calculation. In all cases the scattered positron is excluded. The recombination of particles is done according to the Snowmass convention [15]. The jets are reconstructed as massless.

Each jet has to fulfil $\overline{E}_{T,\mathrm{Breit}} > 5$ GeV and must lie in the acceptance of the LAr calorimeter, i.e. the pseudorapidity[2] of the jets $\eta_{jet,lab}$ in the laboratory frame required to lie within $-1 < \eta_{jet,lab} < 2.5$. Starting from 706407 DIS events in the sample for $5 < Q^2 < 100\ \mathrm{GeV}^2$, 2465 events with at least three jets are left. In the high Q^2 sample 30668 DIS events are selected. 666 events survive after the jet cuts. These numbers include the requirement $M_{\mathrm{3jet}} > 25$ GeV.

4 The Definition of the Observables

Inclusive three jet cross sections are measured as a function of Q^2, the Bjorken-scaling variable x_{Bj}, the three jet invariant mass (M_{3jet}) and the mean transverse energy of the jets in the Breit frame ($\overline{E}_{T,\mathrm{Breit}}$). For the cross sections as a function of x_{Bj} and Q^2 an additional requirement that $M_{\mathrm{3jet}} > 25$ GeV is made.

Shape normalised topological variables are defined in the three jet centre of mass system (3-jet CMS). For a given three jet mass M_{3jet} and for massless jets five dimensionless variables fully characterise the properties of the three jet system. We follow the definitions proposed in [16] for $p\bar{p}$ collisions. Two variables specify the sharing of the available energy and two variables fix the orientation of the three-jet system with respect to the beam direction. The last variable is an overall azimuthal angle and is not considered here.

[2]The pseudo-rapidity η is defined as $\eta \equiv -\ln(\tan\theta/2)$ where θ is the polar angle with respect to the proton direction. This definition is chosen in both the laboratory frame and the Breit frame.

It is convenient to label the two incoming partons with 1 and 2 and the three outgoing partons or jets with 3, 4 and 5. The final state jets are ordered by energy starting with index 3 for the most energetic jet, i.e. $E_3 > E_4 > E_5$. The energy of the jets can be expressed in scaled variables (Dalitz-variables):

$$X_3 = \frac{2\ E_3}{M_{3\mathrm{jet}}}\ ,\ X_4 = \frac{2\ E_4}{M_{3\mathrm{jet}}}. \tag{1}$$

In the 3-jet centre of mass system the invariant three jet mass is given by: $M_{3\mathrm{jet}}\ = E_3+E_4+E_5$. The scaled energy of the least energetic jet is simply given by the scaled energies of the other two by: $X_3 + X_4 + X_5 = 2$. From energy and momentum conservation it follows that the most energetic jet carries at least $1/3$ of the available centre of mass energy, i.e. $2/3 < X_3 < 1$.

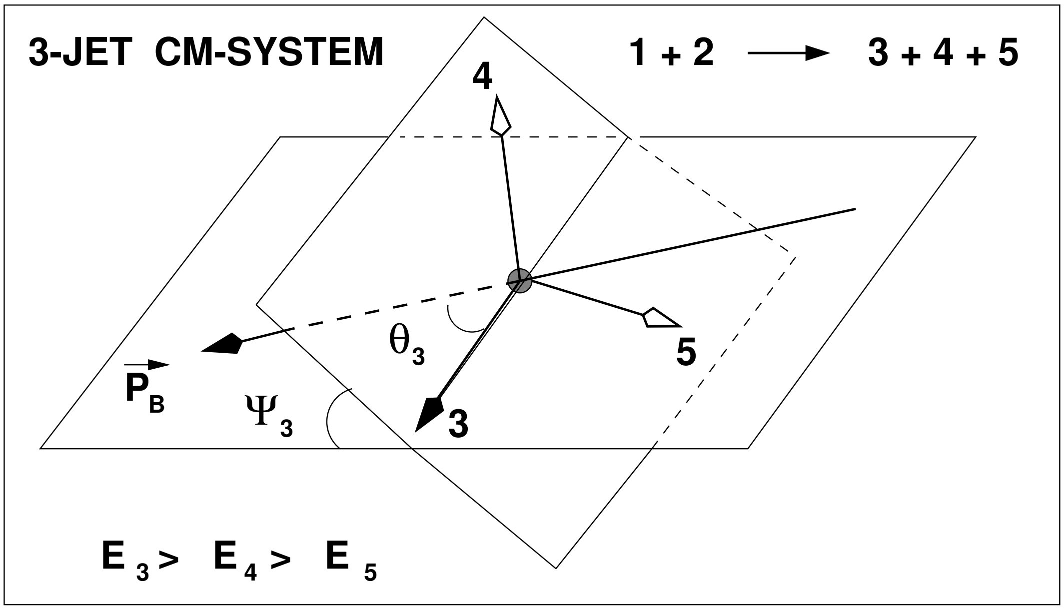

Figure 1: Sketch of a possible configuration in the rest system of the three jet final state. The indices 3, 4, 5 denote the jets ordered in energy and $\vec{P_B}$ refers to the momentum vector of the proton beam. The positive z-axis is defined by the direction of the incoming proton.

Two angles fix the orientation of the jets:

$$\cos\theta_3 = \frac{\vec{P}_B \cdot \vec{P}_3}{\mid \vec{P}_B \mid \mid \vec{P}_3 \mid}\quad ,\quad \cos\Psi_3 = \frac{(\vec{P}_3 \times \vec{P}_B)\cdot(\vec{P}_4 \times \vec{P}_5)}{\mid \vec{P}_3 \times \vec{P}_B \mid \mid \vec{P}_4 \times \vec{P}_5 \mid} \tag{2}$$

where $\vec{P}_i$ ($\vec{P}_B$) denote the jet (proton beam) momentum 3-vectors. θ_3 is the polar angle of the leading jet with respect to the proton beam direction and ψ_3 describes the orientation of the plane spanned by the jets with respect to the plane containing the beam direction and the leading jet. ψ_3 is strongly influenced by the orientation of the least energetic jet. If $\psi_3 \approx 0$ or $\psi_3 \approx \pi$, this jet has been radiated close to the plane containing the beam and the highest energetic jet indicating in most cases a radiation from the strongly interacting hadron in the initial state.

Fig. 1 illustrates the definition of these observables.

5 QCD Monte Carlo Models and QCD Calculations

Simulations of the detailed properties of the hadronic final state are available in the form of Monte Carlo event generators. They include the matrix element of the hard subprocess to first order in the strong coupling constant α_s, approximations of higher order QCD radiation effects, and a model to describe the non-perturbative transition from partons to hadrons.

The LEPTO Monte Carlo [17] incorporates the $\mathcal{O}(\alpha_s)$ QCD matrix elements and approximates the higher order parton emission of partons to all orders in α_s using the concept of parton showers [18] based on the leading logarithm DGLAP equations [19]. QCD radiation can occur before and after the hard subprocess. The formation of hadrons is simulated using the LUND string model [20] as implemented in JETSET [21].

RAPGAP [22] contains the same physics assumptions as LEPTO, but treats the singularities of the $\mathcal{O}(\alpha_s)$ matrix element in a different way.

The HERWIG Monte Carlo [23] also includes the $\mathcal{O}(\alpha_s)$ QCD matrix element, but uses another implementation of the parton shower cascade which takes coherence effects fully into account. The hadronisation is done by the cluster fragmentation model [24].

In ARIADNE [25] gluon emissions are treated by the colour dipole model [26] assuming a chain of independently radiating dipoles spanned by colour connected partons. The first emission in the cascade is corrected to reproduce the matrix elements to first order α_s [27].

DJANGO [28] provides an interface between the event generators LEPTO or ARIADNE and HERACLES [29] which allows to include $\mathcal{O}(\alpha)$ QED corrections at the lepton line.

Perturbative QCD calculations are performed to order $\mathcal{O}(\alpha_s^2)$ using the DISENT program [30] which produces an exact leading order calculation of the three parton final state. The renormalisation and the factorisation scale is set to the mean transverse energy of the jets.

The strong coupling constant is taken to be consistent with that used in the parton density function, CTEQ5L [31], where $\Lambda^5_{QCD} = 0.146$ GeV for five flavours. In the Monte Carlo models CTEQ4L [32] with the corresponding value of $\Lambda^5_{QCD} = 0.181$ GeV is used.

Configurations where the three jets are homogeneously distributed in phase space were generated using a modified version of RAPGAP. This is done by assumimg that the parton from the proton is a gluon with energy distributed according to the gluon density. The three jet mass is then calculated from the four momenta of the gluon and the virtual photon (distributed according to equivalent photon approximation). The three jet final state is generated according to phase space and colour connected with the proton remnant. Optionally, inital and final state parton showers can be added. In this phase-space generator, the hadronisation and parton showers are not used. The mass spectrum of the three parton jets is reweighted to reproduce the three jet mass spectrum of the data.

6 Correction of the Data and Systematic Errors

The data are corrected for detector effects and QED radiation from the incoming and outgoing lepton. The detector response is determined using events from Monte Carlo event generators that were subjected to a detailed simulation of the H1 detector. The RAPGAP, LEPTO and ARIADNE event generators were used. All three programs were interfaced with HERACLES to take QED radiation into account.

The simulated samples give a good description of the kinematic variables of the inclusive DIS data sample and of basic event properties like the overall transverse or longitudinal momentum balance in the event. Also the energy flow around the jets is well described.

The measured data points are corrected bin-by-bin for detector effects. Using the generated event samples, the correction factor for each bin is determined as the ratio of the generated value of the observable (without QED radiation) to the value reconstructed after detector simulation (including QED radiation).

Bin widths were adjusted such that in all bins purities of at least 40% are achieved. This includes the critical migrations from the two jet to the three jet sample.

The dependence of the correction factors on details of the modeling of the hadronic final state is taken into account by considering the difference between the correction factors derived from ARIADNE and RAPGAP (for $5 < Q^2 < 100\ \mathrm{GeV}^2$) and from ARIADNE and LEPTO (for $150 < Q^2 < 5000\ \mathrm{GeV}^2$) as an estimate of the systematic uncertainty.

The measurement was repeated using only energy depositions in the calorimeters instead of the combination of energy depositions and tracks. In the low Q^2 analysis this difference has been included in the systematic error. In the high Q^2 analysis no dependence has been found. Further systematic errors are determined by varying the energy deposits in the calorimeter by 4%. The uncertainty of the energy scale of the scattered positron is assumed to be $\pm 2\%$ if the positron is detected in the backward calorimeter and to be $\pm 0.7 - 3\%$ (depending on polar angle of the scattered positron), if the scattered positron is found in the LAr calorimeter. An additional systematic error comes from the resolution of the angle of the scattered positron. This angle is varied within 1 (3 mrad) for $Q^2 < 100$ GeV ($Q^2 > 150$ GeV). An overall uncertainty of 1.5% from the measurement of the luminosity is also considered. All systematic errors are added in quadrature and included in all results. The inner error bars indicate the statistical errors only.

7 Results

7.1 Three Jet Cross Sections

The three jet cross section as a function of $Q^2$and x_{Bj} for $5 < Q^2 < 5000\ \mathrm{GeV}^2$ is shown in the upper pictures of Fig. 2 and Fig. 3. The cross section falls over four orders of magnitude. The three jet cross section as a function of $M_{\rm 3jet}$ and $\overline{E}_{T,\rm Breit}$ for the two Q^2 regions $5 < Q^2 < 100$ GeV^2 and $150 < Q^2 < 5000\ \mathrm{GeV}^2$ is shown in the lower pictures of Fig. 2 and Fig. 3. In the data the $\overline{E}_{T,\rm Breit}$ as well as the $M_{\rm 3jet}$ spectrum becomes harder for higher Q^2.

The data are compared to leading order $\mathcal{O}(\alpha_s^2)$ pQCD calculations. The data have been only corrected for detector effects. Hadronisation corrections, which have to be applied to the $\mathcal{O}(\alpha_s^2)$ pQCD calculations to compare them with the data, lower the calculated cross sections by about $20-40\%$. The calculation gives a fair description of the data for $Q^2 \gtrsim 40$ GeV^2 and $\overline{E}_{T,\rm Breit} \gtrsim 10-20$ GeV or masses $M_{\rm 3jet} \gtrsim 50$ GeV. As Q^2 and $\overline{E}_{T,\rm Breit}$ decrease the leading order calculations fall below the data. At the lowest Q^2 and $\overline{E}_{T,\rm Breit}$ they undershoot the data by 40%. Given the additional hadronisation corrections of $20-40\%$, they clearly fail to describe the data. It is interesting to note that leading order $\mathcal{O}(\alpha_s)$ calculations also fail to describe the dijet cross sections [1] at low Q^2 and $\overline{E}_{T,\rm Breit}$.

7.2 The Rate of the Three to Two Jet Cross Sections

The ratio of the three jet to the two jet cross section $R_{3/2}$ is shown in Fig. 4 and for $150 < Q^2 < 5000$ GeV^2. For the two jet cross section $M_{2jet} > 25$ GeV and for the three jet cross section $M_{3jet} > 25$ GeV is required. This ensures that the parton distributions in the proton are probed at a similar momentum fraction $\xi = x_{Bj}\ (1 + M^2_{njet}/Q^2\ )$ values. The rate $R_{3/2}$ is approximately flat in Q^2 and with a value of $R_{3/2} = 0.3$. It rises, however, as the mass of the hard subsystem M^2_{njet} increases. Events with three jets exhibit a harder mass spectrum than events with two jets. Perturbative $\mathcal{O}(\alpha_s^2)$ calculations give a fair description of the data (see Fig.4) given that hadronisation effects lower lower the pQCD rate by about $10-30\%$. With the exception of ARIADNE, also the QCD Monte Carlo models give a reasonable description of these rates as shown in Fig. 5. ARIADNE predicts a rate which is too low. This shows that the parton shower approach is a rather good approximation to the data and to the exact leading order $\mathcal{O}(\alpha_s^2)$ pQCD calculation.

7.3 Topological Variables

The topological variables are shown in Fig. 6 for $5 < Q^2 < 100$ GeV^2 and in Fig. 10 for $150 < Q^2 < 5000$ GeV^2. In order to reduce the influence of the $\overline{E}_{T,\rm Breit}$ cut on the topological variables in the jet rest frame, additional conditions are imposed. In both Q^2 regions it is required that $M_{\rm 3jet} > 25$ GeV. In the low Q^2 region a sufficiently high number of events is available to apply hard cuts on $X_3 < 0.9$ and $\mid \cos\theta_3 \mid < 0.6$. Other possible cut scenarios have also been investigated [33]. In the high Q^2 region only the most obvious regions where the $\overline{E}_{T,\rm Breit}$ cut completely depopulates the phase space can be removed. Here $X_3 < 0.95$ and $\mid \cos\theta_3 \mid < 0.8$ is demanded.

All four variables X_3, X_4, $\cos\theta_3$ and Ψ_3 are described by pQCD calculations as shown in Fig. 6 and Fig. 10. Since these observables are shape normalised, they are less affected by hadronisation corrections (below 10%). Also shown are the distributions from three jets which are uniformly distributed in the available phase space (see Fig. 6 dashed line). The pQCD and phase space distributions of the Dalitz variables X_3 and X_4 are very similar but, at low Q^2, the distributions of $\cos\theta_3$ and Ψ_3 are distinct. This is most pronounced for the Ψ_3 distribution. The $\overline{E}_{T,\rm Breit}$ requirement strongly suppresses configurations where the least energetic jet is emitted in the direction of the incoming proton. The largest phase space is available for events where the least energetic jet is emitted orthogonal to the beam direction. However, the data behave in the opposite way. They follow the predicted QCD radiation pattern. The least energetic jet is most likely to be radiated close to the plane containing the proton and the highest energetic jet. In the high Q^2 region this effect is masked by the remaining influence of the $\overline{E}_{T,\mathrm{Breit}}$ cut. Here data, pQCD calculation and the phase space lead to similar distributions. However, using the DISENT program it has been verified that by lowering the $\overline{E}_{T,\mathrm{Breit}}$ cut or by applying the same hard cuts on X_3 and $\cos\theta_3$ as in the low Q^2 analysis similar conclusions could be drawn [34].

The QCD Monte Carlo models give a fair description of the shape normalised topological variables (see Fig. 7 and Fig. 11). Within the parton shower models, it is possible to separate contributions from initial and final state radiation. As can be seen in Fig. 8 the overwhelming part of the three jet cross sections is caused by inital state radiation. It is interesting that the Ψ_3 distribution behaves very differently when on top of the $\mathcal{O}(\alpha_s)$ matrix elements only either radiation from the parton in the initial state or from the final state partons produced in the hard scattering is allowed. This is shown in Fig. 9. When only final state radiation is allowed there is no prefered Ψ_3 angle and the distribution is close to that from phase space alone. Only inital state radiation gives a Ψ_3 distribution which prefers angles close to the proton beam. We conclude that the least energetic jet is predominantly caused by initial state radiation from the strongly interacting parton in the proton.

8 Summary

The cross sections for three jets at high transverse energy have been measured for $5 < Q^2 < 5000\ \mathrm{GeV}^2$ in DIS at HERA as a function of the Bjorken scaling variable x_{Bj}, the photon virtuality Q^2, the mean transverse jet energy $\overline{E}_{T,\mathrm{Breit}}$ and the invariant jet $M_{3\mathrm{jet}}$. $\mathcal{O}(\alpha_s^2)$ pQCD calculations are only able to describe the cross sections, if Q^2 is relatively large ($Q^2 \gtrsim 40\ \mathrm{GeV}^2$) and $\overline{E}_{T,\mathrm{Breit}}$ is not too small ($\overline{E}_{T,\mathrm{Breit}} \gtrsim 10 - 20$ GeV). At low Q^2 and low $\overline{E}_{T,\mathrm{Breit}}$ they clearly fall below the data.

The ratio of the two to the three jet cross section has been measured for $150 < Q^2 < 5000\ \mathrm{GeV}^2$. $\mathcal{O}(\alpha_s^2)$ pQCD calculations and parton shower Monte Carlo models give a fair description of the data.

The shape normalised variables characterising the topology of the jets in the three jet rest frame have been measured for $5 < Q^2 < 5000\ \mathrm{GeV}^2$. The angular orientations of the three jets follow the expected pattern from pQCD. Both $\mathcal{O}(\alpha_s^2)$ pQCD calculations and parton shower models are consistent with the data. At low Q^2 additional hard cuts have been placed to reduce the influence of the $\overline{E}_{T,\mathrm{Breit}}$ requirement to the available phase space. Here, the least energetic jet is most likely radiated in the proton beam direction. This is inconsistent with a uniform population of the jets in the phase space, but expected from $\mathcal{O}(\alpha_s^2)$ pQCD. Within the QCD models incorporating $\mathcal{O}(\alpha_s)$ matrix elements and parton showers the dominant production mechanism of the three jet events is initial state radiation from a parton in the proton. The observed radiation pattern of the least energetic jet is consistent with initial state radiation, but very distinct from final state radiation.

References

[1] H1 Collab., C. Adloff et al., XXIX Int. Conf. on HEP, paper: 520, Vancouver (Canada) 1998 .

[2] UA1 Collab., G. Arnison et al., Phys. Lett. B 158 (1985) 494 .

[3] UA2 Collab., J.A. Appel et al., Z. Phys. C 30 (1985) 341 .

[4] CDF Collab., F. Abe et al., Phys. Rev. D 45 (1992) 1448 .

[5] CDF Collab., F. Abe et al., Phys. Rev. Lett. 75 (1995) 608 .

[6] CDF Collab., F. Abe et al., Phys. Rev. D 54 (1996) 4221 .

[7] D0 Collab,, S. Abachi et al., Phys. Rev. D 53 (1996) 6000 .

[8] ZEUS Collab., J. Breitweg et al. , Phys. Lett. B 443 (1998) 394 .

[9] H1 Collab., C. Adloff et al., DESY–98–076, Hamburg (Germany) 1998, submitted to Eur. Phys. J. .

[10] H1 Collab., C. Adloff et al., DESY-98-205 Hamburg (Germany) 1998, submitted to Eur. Phys. J. C .

[11] H1 Collab., C. Adloff et al., Measurement of Neutral and Charged Current Cross Sections in Positron-Proton Collisions at Large Momentum Transfer, in preparation .

[12] R. Engel, Z. Phys. C 66 (1995) 203; R. Engel and J. Ranft, Phys. Rev. D 54 (1996) 4244 .

[13] S. D. Ellis and D. E. Soper, Phys. Rev. D 48 (1993) 3160 .

[14] S. Catani, Yu. L. Dokshitzer, M.H. Seymour and B.R. Webber, Nucl. Phys. B 406 (1993) 347 .

[15] J. Huth et al., Proceedings of the Summer Study on High Energy Physics, Snowmass, Colorado (1990) 134 .

[16] S. Geer, T. Asakawa, Phys. Rev. D 53 (1996) 4793 .

[17] G. Ingelman, A. Edin and J. Rathsman, Comp. Phys. Comm. 101 (1997) 108; version used: 6.5 .

[18] M. Bengtsson and T. Sjöstrand, Z. Phys. C 37 (1998) 465 .

[19] V.N. Gribov and L.N. Lipatov, Sov. J. Nucl. Phys. 15 (1972) 438 and 675;
Yu.L. Dokshitzer, Sov. Phys. JETP 46 (1977) 641;
G. Altarelli and G. Parisi, Nucl. Phys. 126 (1977) 297 .

[20] B. Andersson et al., Phys. Rep. 97 (1983) 31 .

[21] T. Sjöstrand, Comp. Phys. Comm. 39 (1986) 347; T. Sjöstrand and M. Bengtsson, ibid. 43 (1987) 367 .

[22] H. Jung, Comp. Phys. Comm. 86 (1995) 147 (version used 2.08) .

[23] G. Marchesini et al., Comp. Phys. Comm. 67 (1992) 465; version used: 5.9 .

[24] B.R. Webber, Nucl. Phys. B 238 (1984) 492 .

[25] L. Lönnblad, Comp. Phys. Comm. 71 (1992) 15; version used: 4.08 .

[26] G. Gustafson and U. Petterson, Nucl. Phys. B 306 (1988);
G. Gustafson, Phys. Lett. B 175 (1986) 453;
B. Andersson, G. Gustafson, L. Lönnblad and U. Petterson, Z. Phys. C 43 (1989) 625 .

[27] L. Lönnblad, Z. Phys. C 65 (1995) 285 .

[28] K. Charchula, G. Schuler and H. Spiesberger, Comp. Phys. Comm. 81 (1994) 381; version used: 6.2 .

[29] A. Kwiatkowski, H. Spiesberger and H.-J. Möhring, Comp. Phys. Comm. 69 (1992) 155 .

[30] S. Catani and M.H. Seymour, Nucl. Phys. B 485 (1997) 291, Erratum-ibid. B 510 (1997) 503 .

[31] CTEQ Collab., H.L. Lai et al., MSU-HEP/903100 and hep-ph/9903282 .

[32] CTEQ Collab., H.L. Lai et al., Phys. Rev. D 55 (1997) 1280 .

[33] R. Mohr, Phd-thesis, University of Hamburg, Germany, in preparation .

[34] A. Heister, Diploma-thesis, University of Aachen, Germany, June 1999 .

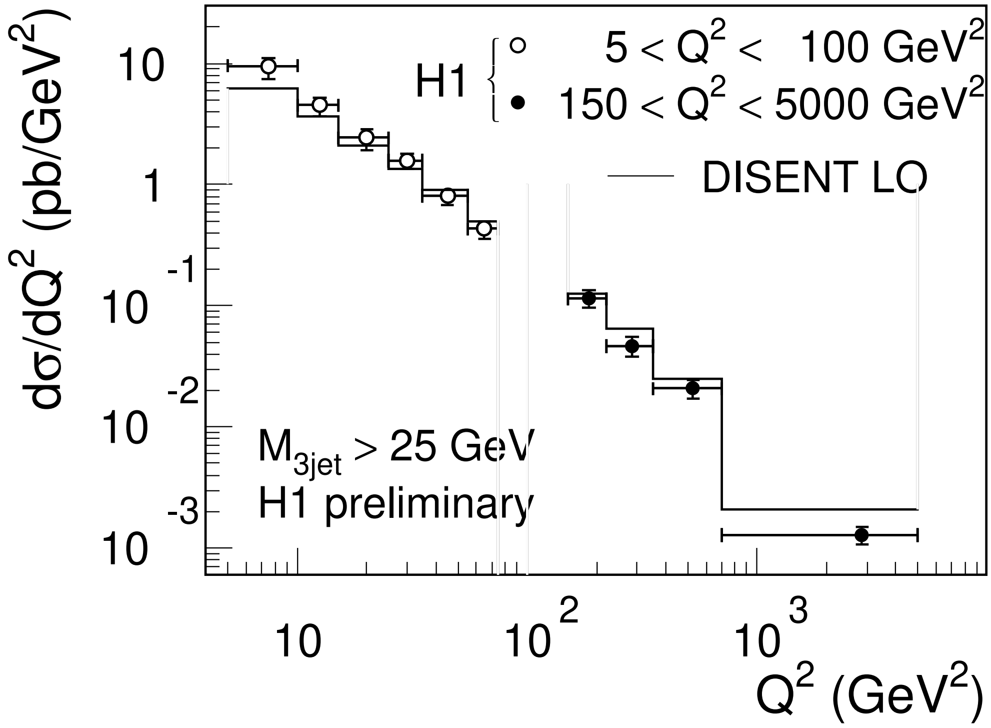

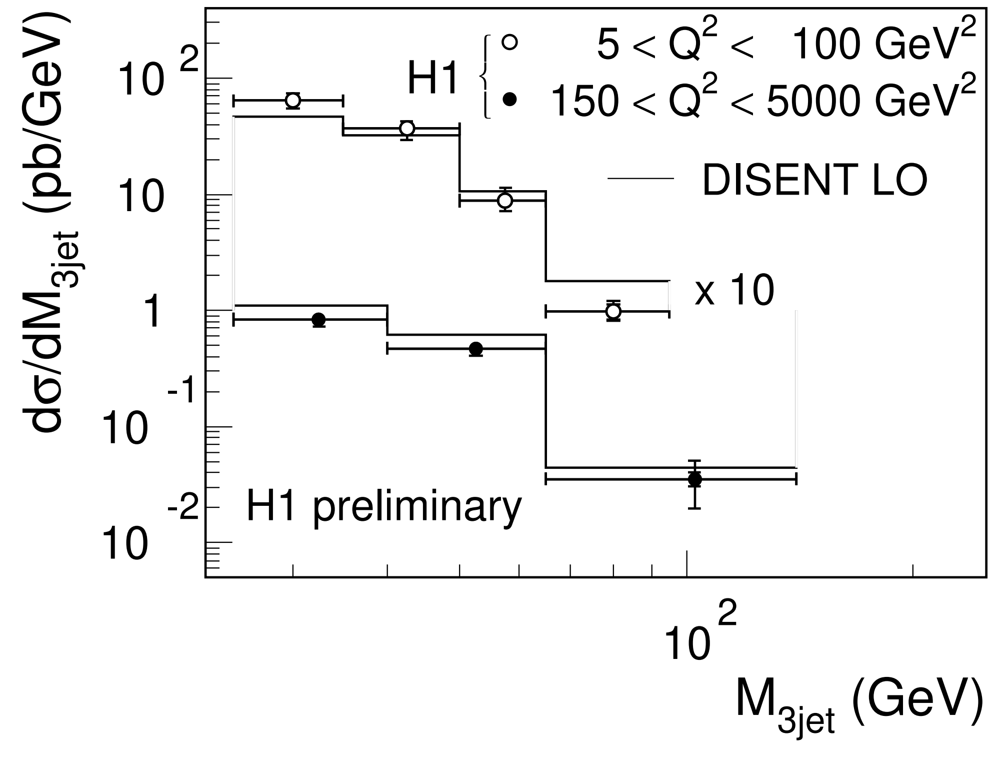

Figure 2: Three jet cross sections for the $5 < Q^2 < 5000$ GeV^2 region as a function of Q^2 (upper figure) and the invariant mass $M_{3\mathrm{jet}}$ (lower figure). For $d\sigma/dM_{3\mathrm{jet}}$ the data at lower Q^2 have been multiplied by a factor of 10. Data are compared to $\mathcal{O}(\alpha_s^2)$ perturbative QCD calculation obtained by the DISENT program. Hadronisation corrections typically lower the NLO prediction by $20 - 30\%$.

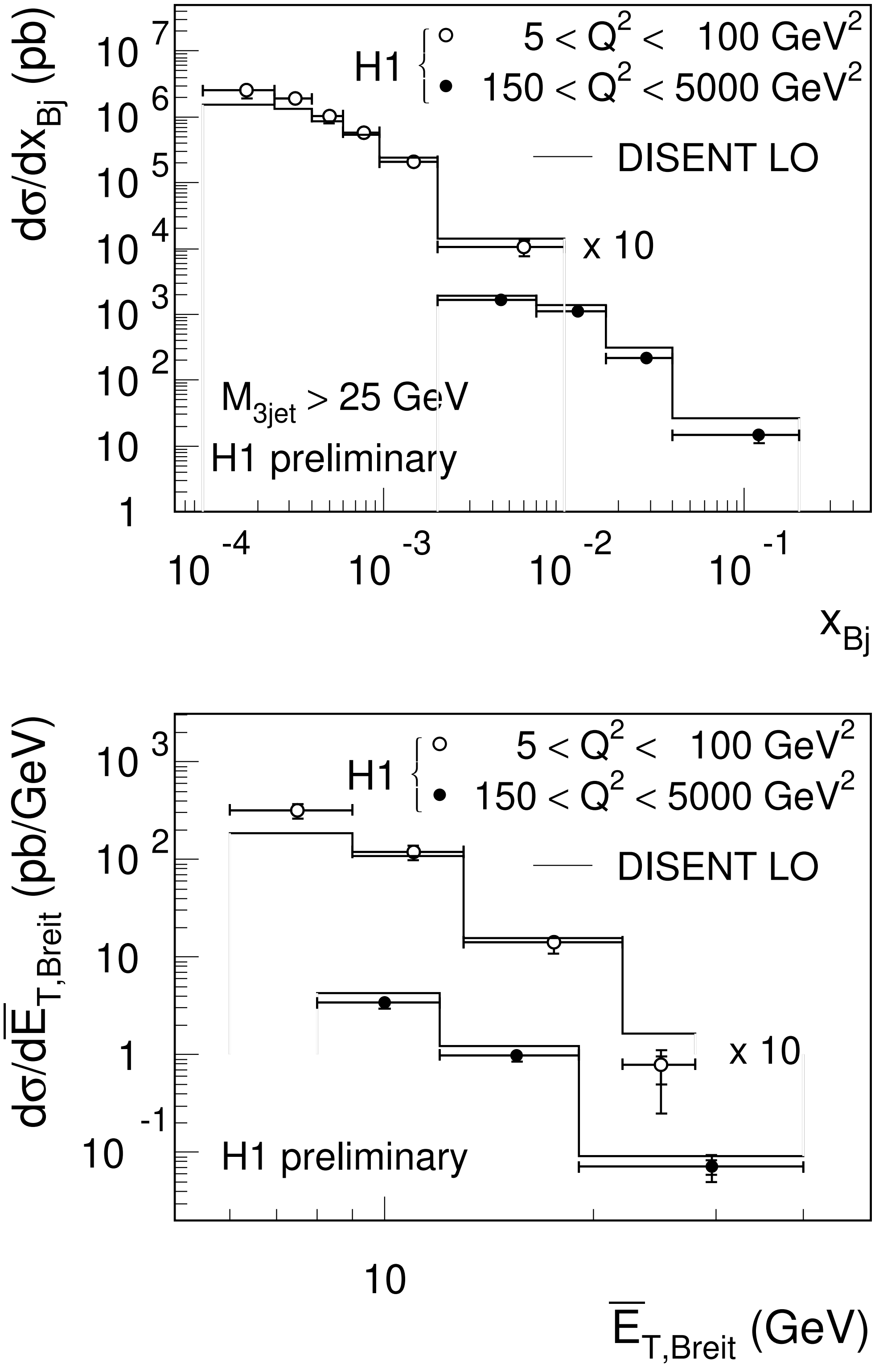

Figure 3: Three jet cross sections for the $5 < Q^2 < 5000\ \mathrm{GeV}^2$ region as a function of x_{Bj} (upper figure) and mean transverse energy of the jets $\overline{E}_{T,\mathrm{Breit}}$ (lower figure). For $d\sigma/d\overline{E}_{T,\mathrm{Breit}}$ and $d\sigma/dx_{Bj}$ the data at lower Q^2 have been multiplied by a factor of 10. Data are compared to $\mathcal{O}(\alpha_s^2)$ perturbative QCD calculation obtained by the DISENT program. Hadronisation corrections typically lower the NLO prediction by $20 - 30\%$.

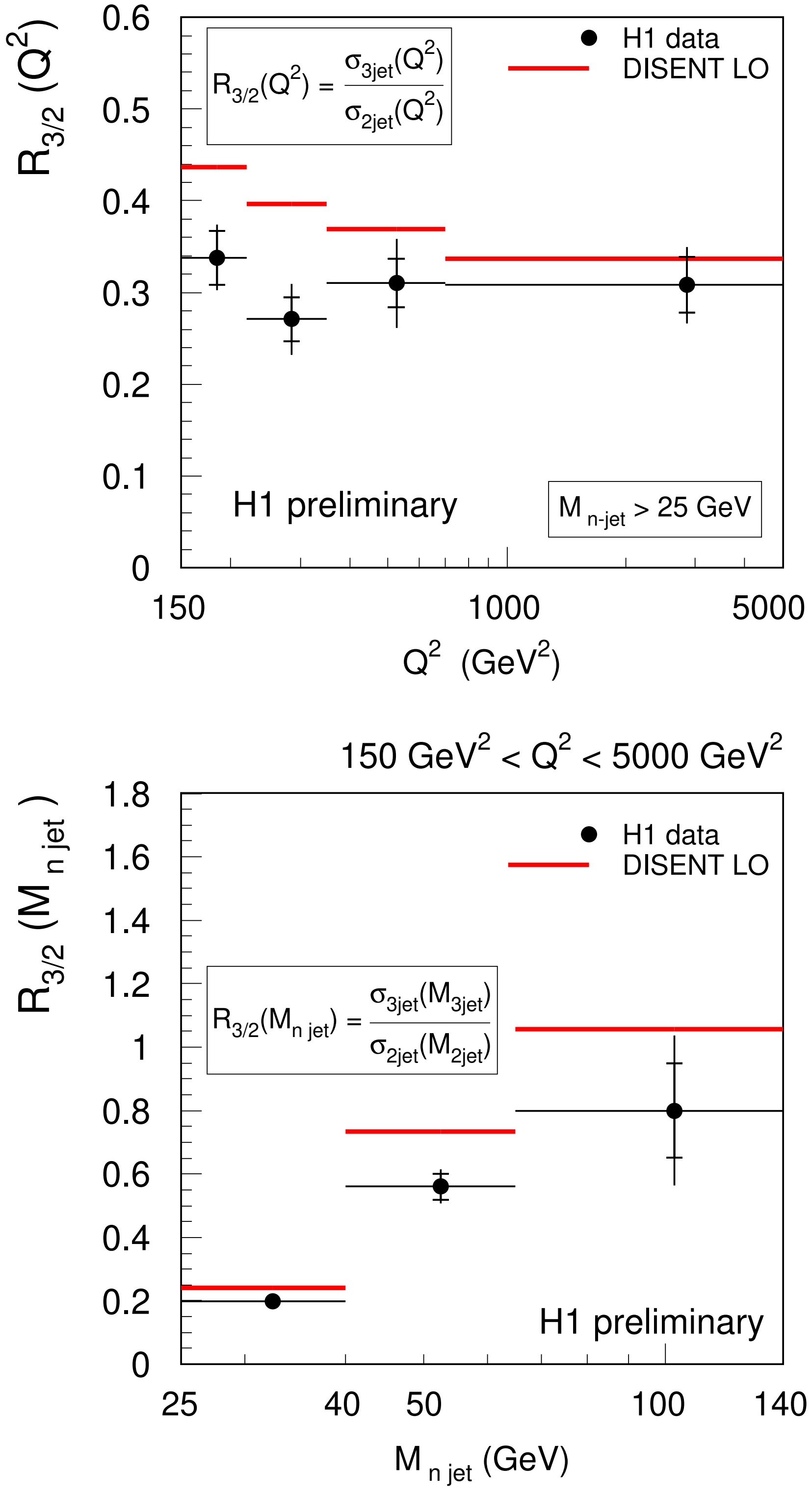

Figure 4: The ratio of the three jet cross section and the two jet cross section $R_{3/2}$ as a function of Q^2 and the mass of the hard process $M_{\rm njet}$ for $150 < Q^2 < 5000\ {\rm GeV}^2$. Data are compared to $\mathcal{O}(\alpha_s^2)$ perturbative QCD calculations obtained by the DISENT program. Hadronisation correction lower the pQCD calculation by $10 - 30\%$.

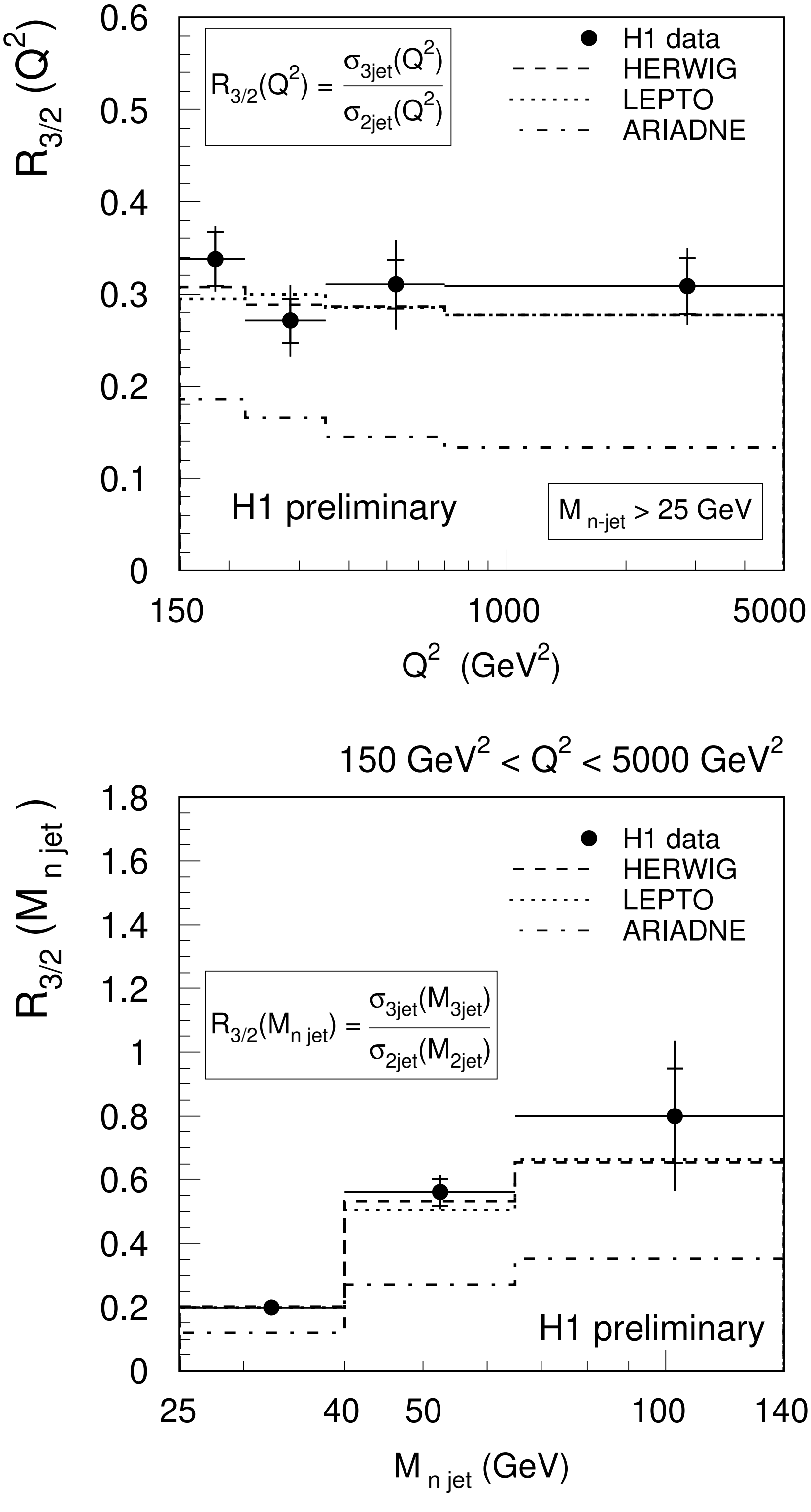

Figure 5: The ratio of the three jet cross section and the two jet cross section $R_{3/2}$ as a function of Q^2 and the mass of the hard process $M_{\rm njet}$ for $150 < Q^2 < 5000\ {\rm GeV}^2$. Data are compared to $\mathcal{O}(\alpha_s^2)$ perturbative QCD calculations obtained by the DISENT program. Hadronisation correction lower the pQCD calculation by $10-30\%$.

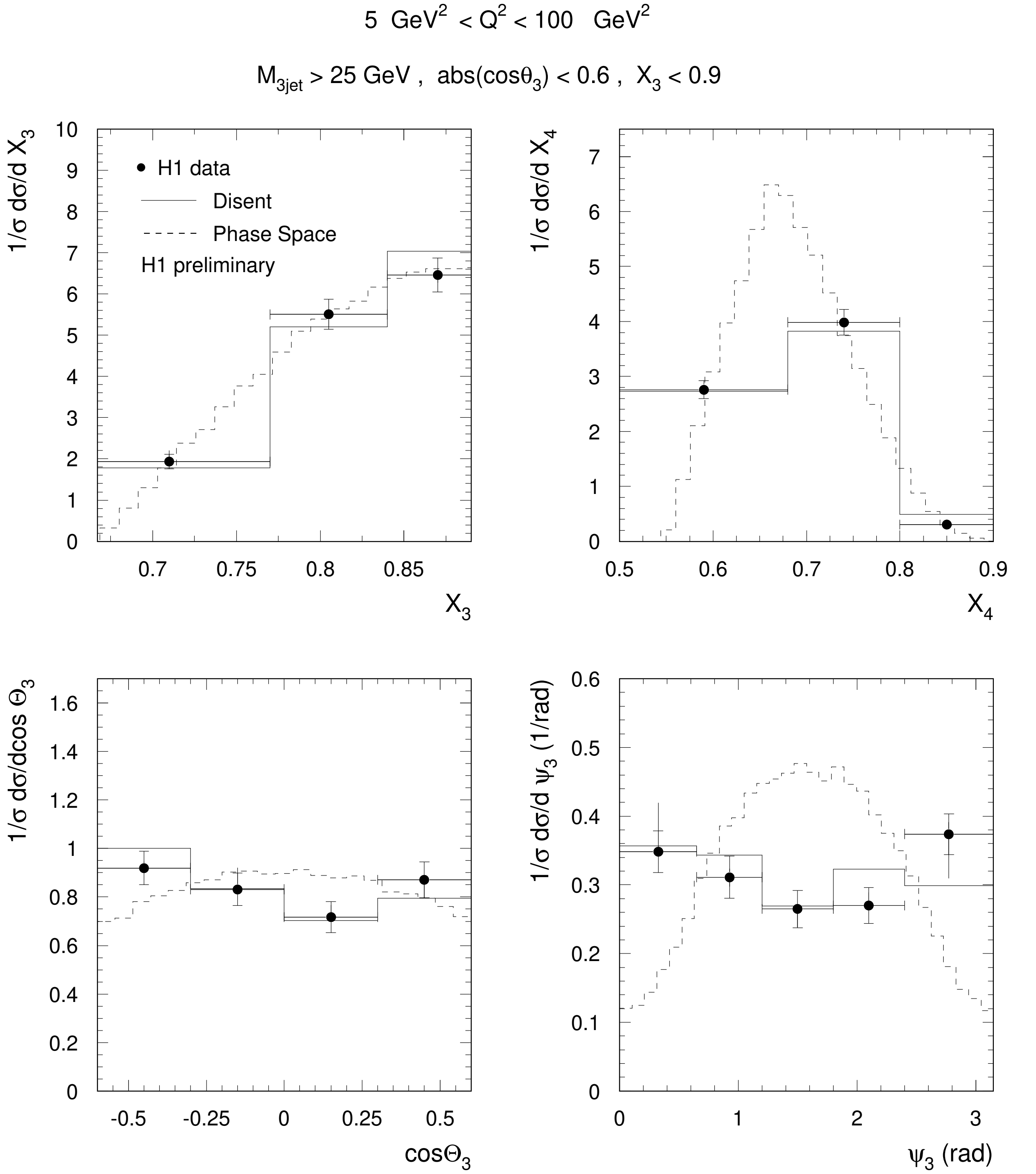

Figure 6: The Dalitz variable $X_3 = 2\,E_3/M_{3\mathrm{jet}}$ and $X_4 = 2\,E_4/M_{3\mathrm{jet}}$, the angle of the highest energetic jet with respect to the proton $\cos\theta_3$ and the angle between the plane containing the first jet and the proton and the plane containing all three jets ψ_3 . All variables are defined in the three jet centre of mass system. The data in the region $5 < Q^2 < 100\ \mathrm{GeV}^2$ are compared to a $\mathcal{O}(\alpha_s^2)$ perturbative QCD calculation obtained by the DISENT program and to a curve illustrating the homogenous distribution of the jets in the pure phase space. Hadronisation correction are flat and lower the pQCD calculation by about 10%.

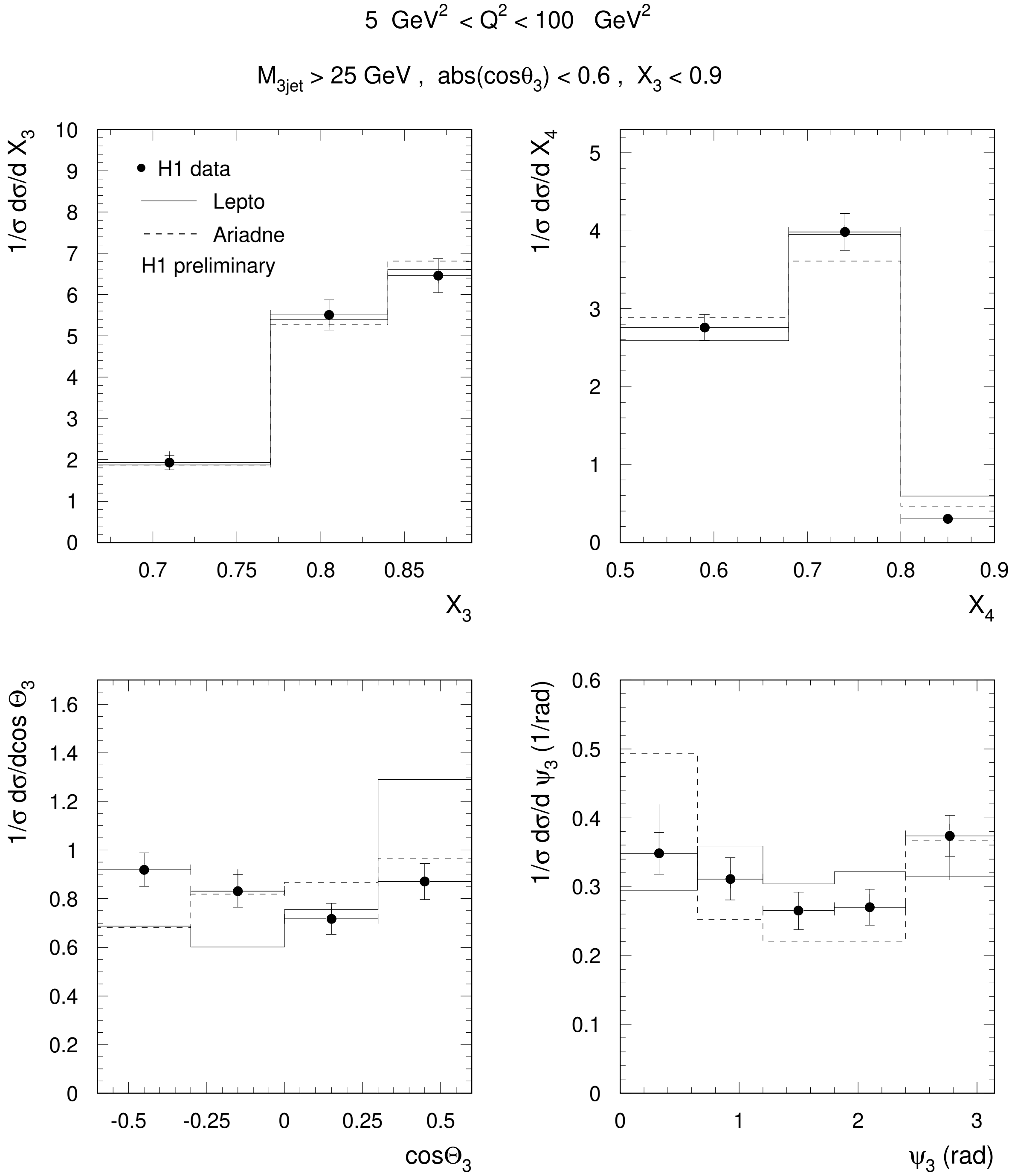

Figure 7: The Dalitz variable $X_3 = 2\,E_3/M_{3\text{jet}}$ and $X_4 = 2\,E_4/M_{3\text{jet}}$, the angle of the highest energetic jet with respect to the proton $\cos\theta_3$ and the angle between the plane containing the first jet and the proton and the plane containing all three jets ψ_3. All variables are defined in the three jet centre of mass system. The data in the region $5 < Q^2 < 100\ \mathrm{GeV}^2$ are compared to Monte Carlo predictions from LEPTO (solid line) and ARIADNE (dashed line).

5 GeV^2 < Q^2 < 100 GeV^2

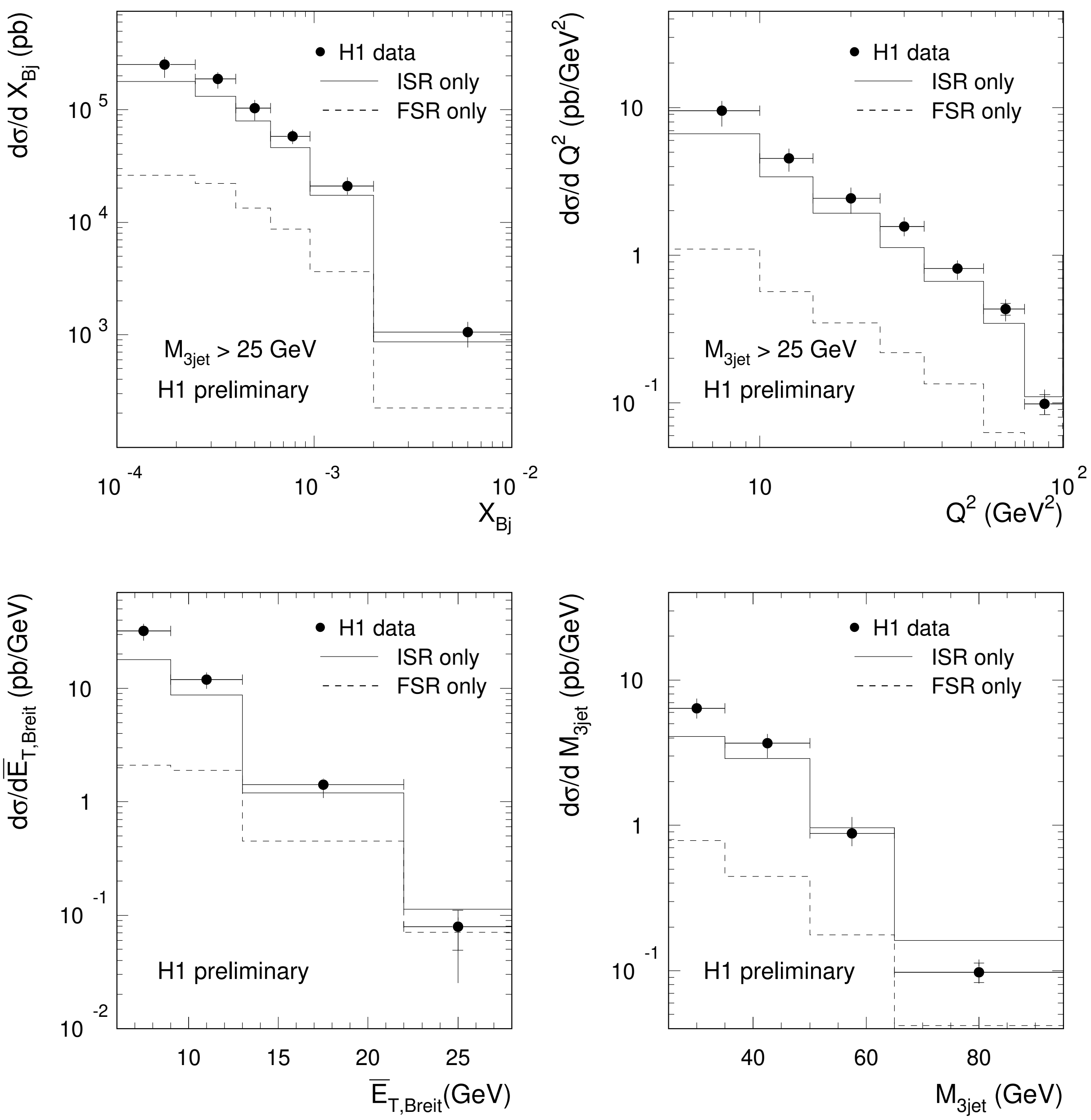

Figure 8: Three jet cross sections for the $5 < Q^2 < 100$ GeV region as a function of x_{Bj} , Q^2 , the invariant mass $M_{3\mathrm{jet}}$ and mean transverse energy of the jets $\overline{E}_{T,\mathrm{Breit}}$. Data are compared to QCD Monte Carlo model predictions from LEPTO adding either only initial state or only final state QCD radiation to the $\mathcal{O}(\alpha_s^2)$ matrix elements.

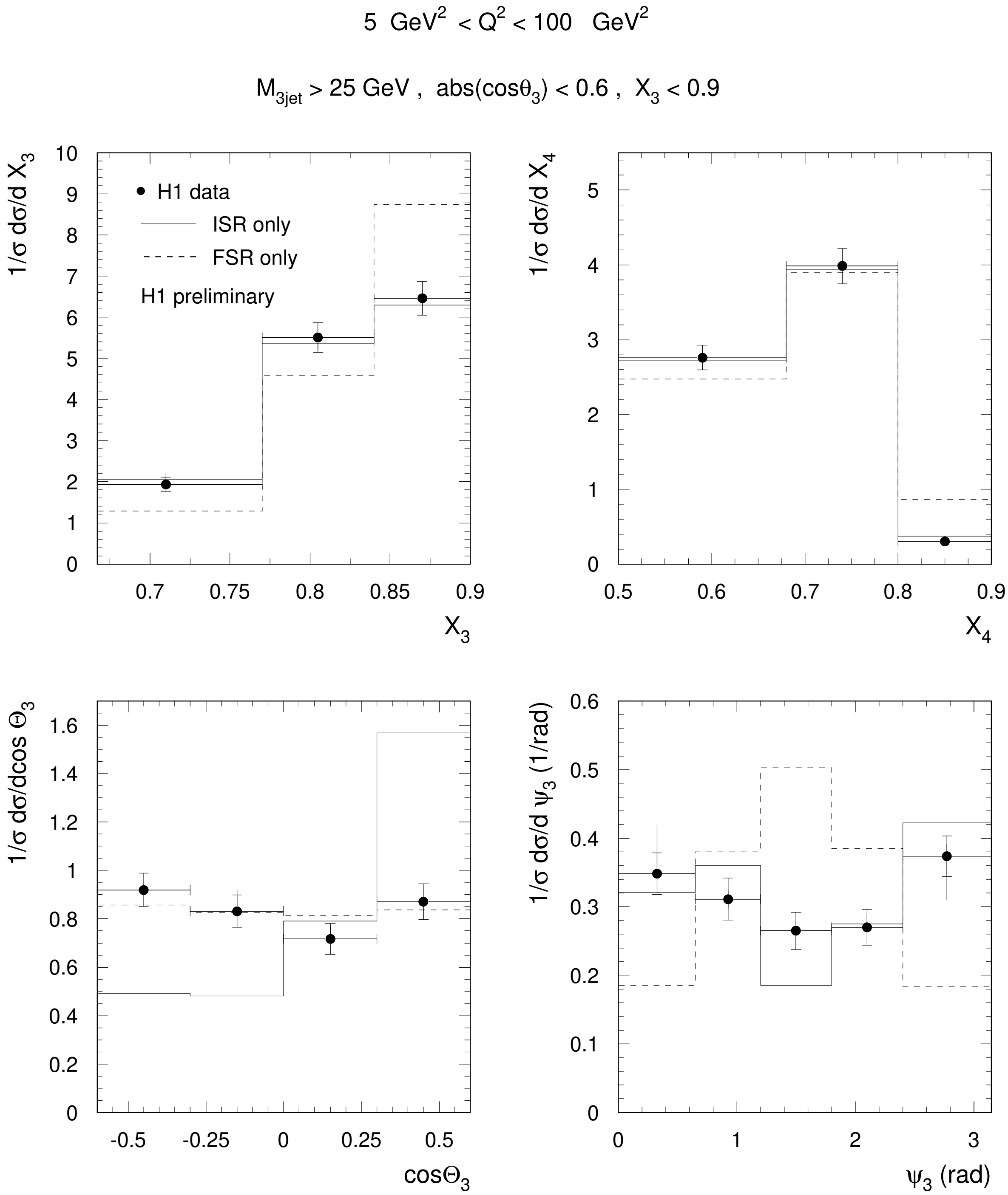

Figure 9: The Dalitz variable $X_3 = 2\,E_3/M_{3\mathrm{jet}}$ and $X_4 = 2\,E_4/M_{3\mathrm{jet}}$, the angle of the highest energetic jet with respect to the proton $\cos\theta_3$ and the angle between the plane containing the first jet and the proton and the plane containing all three jets ψ_3 . All variables are defined in the three jet centre of mass system. Data are compared to QCD Monte Carlo model predictions from LEPTO adding to the $\mathcal{O}(\alpha_s)$ matrix element either only initial or only final state QCD radiation.

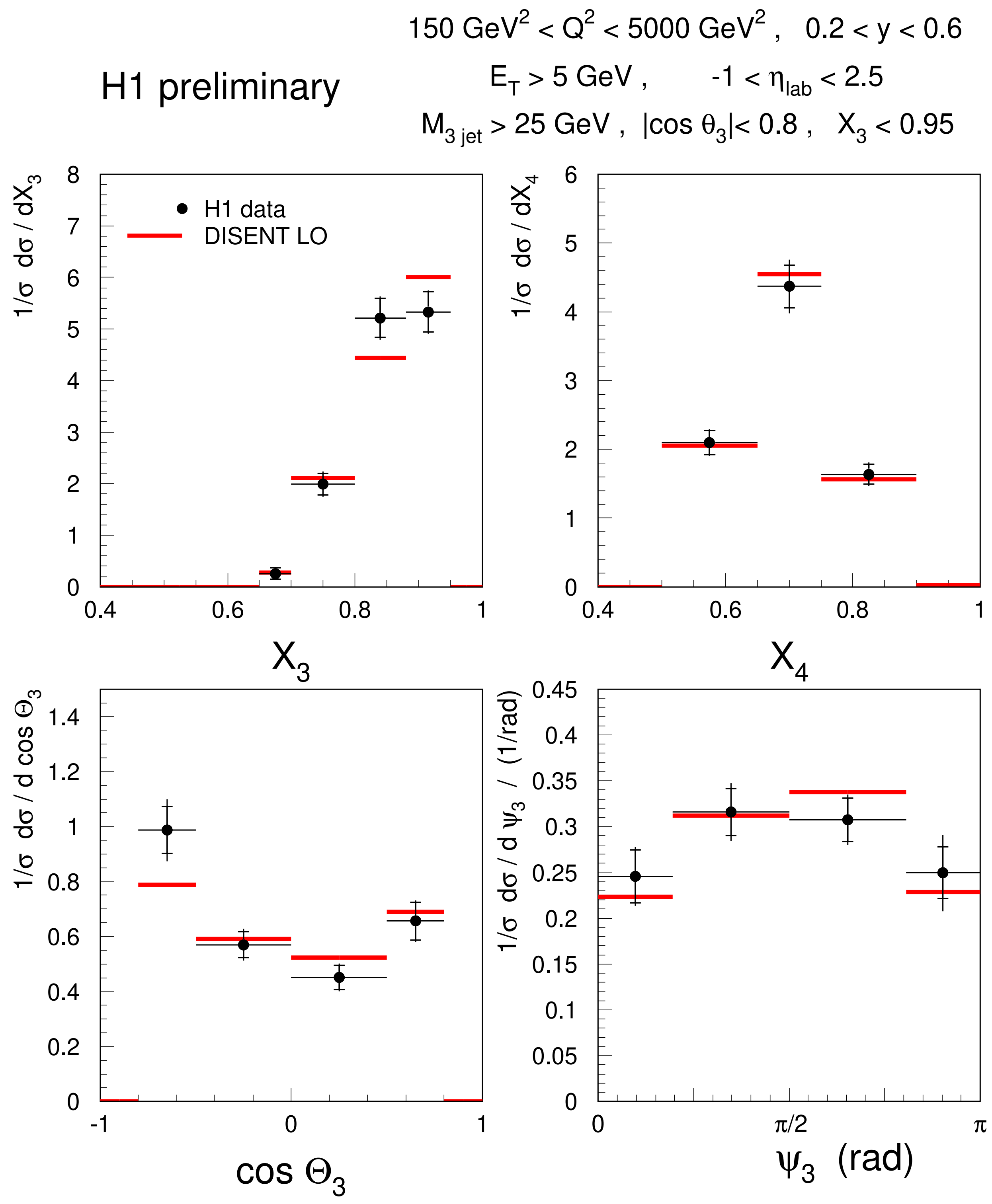

Figure 10: The Dalitz variable $X_3 = 2\,E_3/M_{3\mathrm{jet}}$ and $X_4 = 2\,E_4/M_{3\mathrm{jet}}$, the angle of the highest energetic jet with respect to the proton $\cos\theta_3$ and the angle between the plane containing the first jet and the proton and the plane containing all three jets ψ_3 . All variables are defined in the three jet centre of mass system. The data in the region $150 < Q^2 < 5000\ \mathrm{GeV}^2$ are compared to $\mathcal{O}(\alpha_s^2)$ pQCD calculations

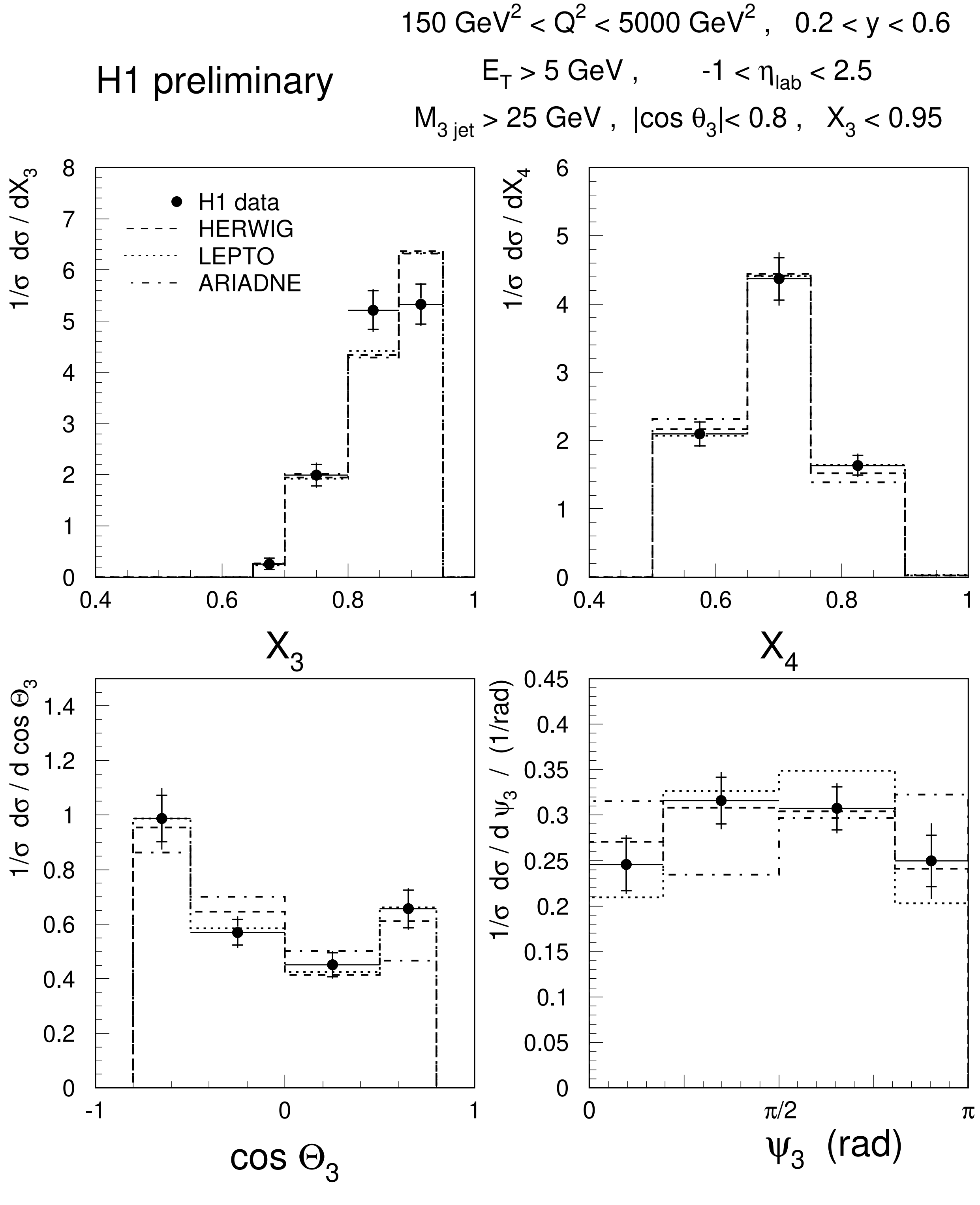

Figure 11: The Dalitz variable $X_3 = 2\,E_3/M_{3\mathrm{jet}}$ and $X_4 = 2\,E_4/M_{3\mathrm{jet}}$, the angle of the highest energetic jet with respect to the proton $\cos\theta_3$ and the angle between the plane containing the first jet and the proton and the plane containing all three jets ψ_3 . All variables are defined in the three jet centre of mass system. The data in the region $150 < Q^2 < 5000\ \mathrm{GeV}^2$ are compared to QCD Monte Carlo models.